Axial Detonation Propagation in an Annular Cylinder of the TATB-Based Explosive PBX 9502

Gabriel A. Montoya, Mark Short, Eric K. Anderson and Stephen J. Voelkel
Shock and Detonation Physics, Los Alamos National Laboratory,
Los Alamos, NM 87545, USA

1 Introduction

In condensed-phase high explosives (HEs), a detonation consists of a shock wave supported by a finite region of chemical reaction where solid reactants are converted into high-pressure products. Detonation speeds in HEs can reach multiple kilometers per second, with associated Chapman-Jouguet (CJ) pressures on the order of tens of gigapascals [1].

The one-dimensional idealization of a detonation is the Zeldovich-von Neumann-Döring (ZND) structure [2]. When propagating at the CJ speed, the subsonic flow behind the shock is accelerated to sonic at the end of the reaction zone, isolating the detonation reaction zone from disturbances originating behind the sonic point [1]. In multi-dimensional detonating HEs, the flow behind the shock expands laterally due to the high pressures in the reaction and product zones. In a cylindrical charge, this causes the shock to become divergently curved, and in response, the flow sonic plane moves into regions of incomplete reaction [3–5]. After a relaxation period, the detonation propagates steadily. The region between the detonation shock and sonic plane is known as the detonation driving zone (DDZ) [5, 6]. Only energy released within the DDZ serves to drive the motion of the detonation. In general, any property that affects the structure and energy release within the DDZ, such as the reaction rate, HE geometry or type of confinement [5], will influence detonation propagation.

Simulations of reactive burn models for detonation propagation that resolve the structure of the DDZ are expensive due to the scale disparity between a typical reaction zone thickness and the geometry scale. Detonation shock dynamics (DSD) models for calculating detonation motion reproduce the influence of the DDZ by propagating a surface in which the normal surface speed is specified as a function of its local curvature [7]. For a given HE, its DSD model is typically calibrated using timing and detonation shock shape data from a series of cylindrical rate-stick geometry tests with varying diameters. The DSD model can be used to study detonation motion in a variety of geometries, such as two-dimensional planar slabs and circular arcs [5, 8, 9]. Here, we study the properties of steady, axial detonation propagation in an annular cylinder of PBX 9502 using a DSD approach. PBX 9502 is an insensitive high explosive containing 1,3,5-triamino-2,4,6-trinitrobenzene (TATB) as the HE crystal, bonded with Kel F-800 or FK-800 [10], a co-polymer of chloro-trifluoro-ethylene and vinylidene-fluoride in a 3:1 ratio by weight, with nominally 95 weight percentage (wt.%) TATB and 5 wt.% Kel F-800 (FK-800). It is one of the most extensively studied HEs due to its unique combination of safety and performance properties. We

Correspondence to: short1@lanl.gov

examine the effect of varying annular radii and confinement, and compare to propagation in a solid cylinder. A PBX 9502 DSD model validation experiment is also described for the annular cylinder geometry.

2 Detonation Shock Dynamics for a Two-Dimensional Axisymmetric Annular Cylinder

Assuming a set of level curves given by $f(\mathbf{x}(t), t) = c$, where c is a constant, with the unit normal to each surface given by $\mathbf{n} = \nabla f/|\nabla f|$, the level set evolution equation can be written as

$$\frac{\partial f}{\partial t} + D_n|\nabla f| = 0, \quad D_n = \mathbf{n} \cdot \frac{d\mathbf{x}}{dt}, \tag{1}$$

where $D_n(\mathbf{x}, t)$ is the surface normal speed and related to curvature κ by

$$D_n = D_n(\kappa), \quad \kappa = \nabla \cdot \mathbf{n}, \tag{2}$$

where κ is the total surface curvature.

Now consider an annular cylinder with inner and outer radius R_i and R_e, respectively, with $R_i \leq r \leq R_e$. Specializing to the zero level set curve, $f = z - z_s(r, t) = 0$, we obtain the evolution equations

$$z_{s,t} = D_n(1 + z_{s,r}^2)^{\frac{1}{2}}, \quad \kappa = -\frac{z_{s,rr}}{(1 + z_{s,r}^2)^{\frac{3}{2}}} - \frac{z_{s,r}}{r(1 + z_{s,r}^2)^{\frac{1}{2}}}. \tag{3}$$

The angles between the normals to the detonation shock surface at the edges of the explosive charge and the axial propagation direction are used as the boundary conditions, setting the degree of confinement felt by the detonation wave in the HE. We define ϕ_i as the surface normal angle on the inner arc boundary, ϕ_e as that on the outer arc boundary, while the angle ϕ_s is that for unconfined (sonic) flow. On $r = R_i$, we apply the condition

$$z_{s,r} = -\tan\phi_i, \quad \phi \geq -\phi_s, \tag{4}$$

with $\phi_i < 0$. On $r = R_e$,

$$z_{s,r} = -\tan\phi_e, \quad \phi \leq \phi_s. \tag{5}$$

with a quadratic extrapolation condition for $\phi > \phi_s$. The extrapolation condition mimics supersonic outflow that is observed in the reactive burn solutions, as detailed in [6, 9].

Equations (3)–(5) are solved on a uniform mesh $R_i \leq r \leq R_e$. Second order upwinding is used for the derivative $z_{s,r}$ and combined with central differencing for $z_{s,rr}$. Time integration is via a second-order Heun's method. At $t = 0$, the DSD surface $z_s(r, 0) = 0$ for $R_i \leq r \leq R_e$ is assigned a normal speed of $D_n = D_{CJ}$ and subsequently evolved in time. For the purposes of transitioning smoothly from the initial surface state where $z_{s,r} = 0$ on $r = R_i$ and $r = R_e$, we linearly increase the surface angles on $r = R_i$ and $r = R_e$ from zero to ϕ_i or ϕ_e in time over a duration of 0.1 μs.

The $D_n - \kappa$ relation is taken from the calibrated PBX 9502 DSD model for lot 008 for an initial density of $\rho_0 = 1.893$ g/cm^3 [11], given by

$$D_n(\kappa) = D_{CJ}\left[1 - B\kappa\left(\frac{1 + C_2\kappa}{1 + C_4\kappa}\right)\right], \tag{6}$$

where D_{CJ} is the Chapman-Jouguet (CJ) detonation velocity, and B, C_2, and C_4 are function parameters, with $D_{CJ} = 7.805727$ mm/μs, $B = 6.670720$ mm, $C_2 = 8.590653$ mm, and $C_4 = 223.935644$ mm.

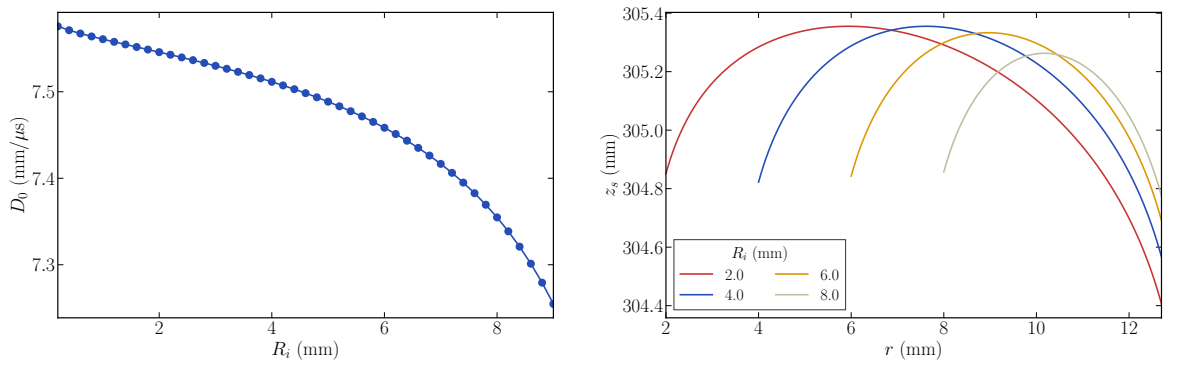

Figure 1: Left (L): Change in D_0 with varying R_i (mm) for $R_e = 12.7$ mm, with $-\phi_i = \phi_e = \phi_s = \pi/6$. Right (R): Corresponding detonation waves shapes for various R_i (mm) and $R_e = 12.7$ mm.

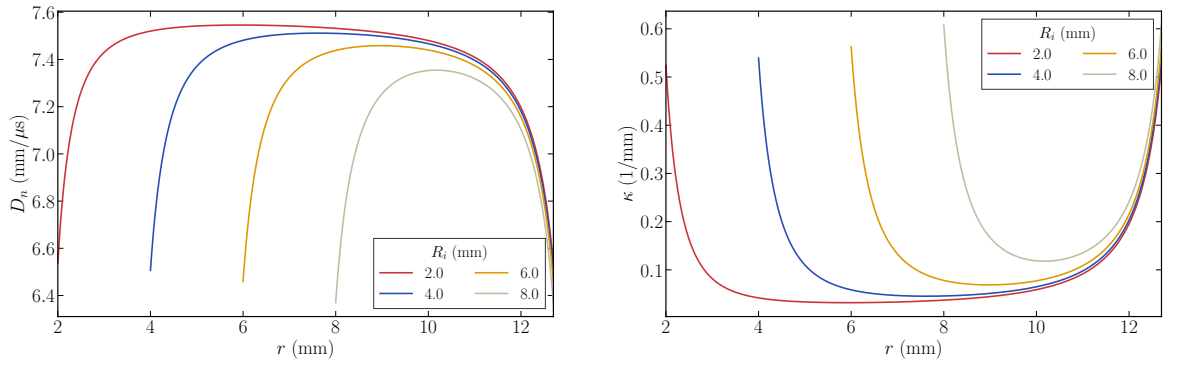

Figure 2: Surface normal speed D_n and curvature κ variations for $R_i \leq r \leq R_e$ for each R_i in Fig. 1R.

As noted, the DSD model can be used be explore a number of facets of detonation propagation in an annular cylinder, such as the effect of varying inner or outer radii, or the effect of confinement on either or both of the inner or outer surfaces. Figure 1L shows the change in D_0 with varying R_i for $R_e = 12.7$ mm in an unconfined charge ($-\phi_i = \phi_e = \phi_s = \pi/6$). For $R_e = 12.7$ mm in a solid cylinder ($R_i = 0$, $\phi_i = 0$), $D_0 = 7.582$ mm/μs. For finite and increasing R_i, the wave speed monotonically decreases as R_i increases. At $R_i = 8.0$ mm, $D_0 = 7.355$ mm/μs. Additionally, the rate of decrease in D_0 increases as R_i increases. For sufficiently large R_i, we expect the detonation will fail as the annulus becomes too thin to support detonation propagation [12]. For reference, in a planar slab of PBX 9502, the failure thickness has been estimated to lie between 3.75 and 4.0 mm [8].

Figure 1R shows corresponding detonation waves shapes for various R_i. The head of the wave moves interior to the annulus for finite R_i due to the unconfined flow on $r = R_i$, in a similar manner observed for an arc configuration [6, 13]. Figure 2 shows the surface normal speed D_n and curvature κ variations for $R_i \leq r \leq R_e$ for each R_i in Fig. 1R. Of particular note are the strong boundary layer variations in D_n and κ near both the inner and outer arc surfaces. Figure 3 shows the diameter effect variation for $R_i = 0$ ($\phi_i = 0$), 5.0 and 10.0 mm. As R_i increases, the diameter effect curves become steeper than for the solid cylinder, while the values of R_e at which low speeds are obtained, e.g., for $D_0 = 7.3$ mm/μs, increases. Figure 4 shows the increase in D_0 that occurs for $R_i = 5.0$ mm and $R_e = 12.7$ mm when the confinement on the inner and outer surfaces becomes stronger, i.e. for decreasing $-\phi_i = \phi_e$.

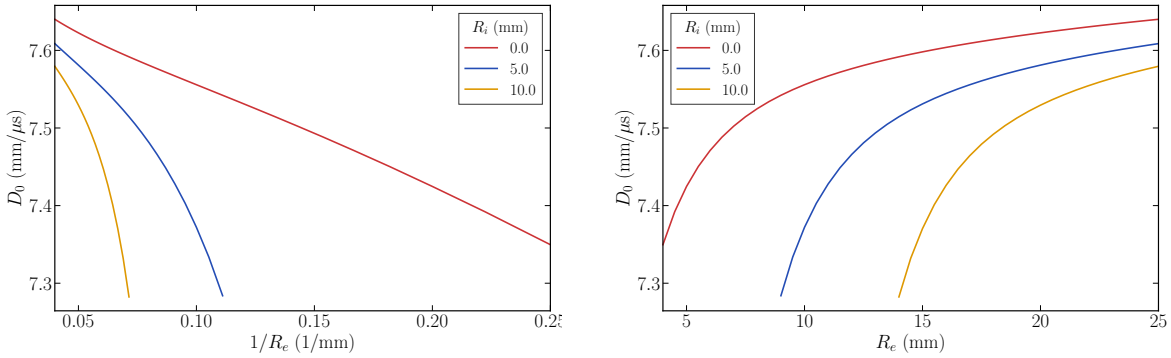

Figure 3: L: Diameter effect curves (D_0 vs. $1/R_e$) for three fixed values of R_i. R: Diameter effect data shown as D_0 vs. R_e.

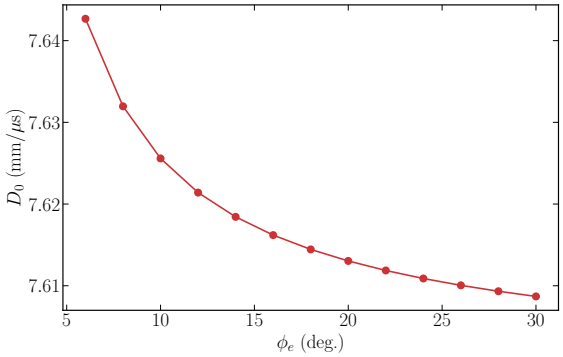

Figure 4: Variation of D_0 with $-\phi_i = \phi_e$ for $R_i = 5.0$ mm and $R_e = 12.7$ mm.

3 PBX 9502 Annulus Geometry Experiment

A validation experiment on the annular cylinder geometry has also been conducted (Fig. 5). The inner radius $R_i = 6.73$ mm and outer radius $R_e = 12.71$ mm, with initial density $\rho_0 = 1.893$ g/cm^3. Twelve 25.4 mm long pellets were used to assemble the test [14]. The inner section of the cylinder was filled with sylgard elastomer to prevent jetting. The elastomer is sufficiently weak that it does not provide any confinement for the detonation [5]. The assembly was initiated with an RP-1 detonator, and boosted by a 25.4 x 25.4 mm cylinder of HMX-based PBX 9501. The steady axial detonation speed (D_0) was measured via ionization wire time-of-arrival diagnostics, in which a linear least squares fit through the time-of-arrival and wire-position data was used to obtain D_0 [14]. The times of arrival of the detonation front as a function of position along a diameter chord at the downstream breakout surface of the annular charge were obtained via a mirror destruction technique and recorded on a streak camera [14].

The steady detonation speed in the annular cylinder experiment was calculated to be $D_0 = 7.422$ mm/μs. The DSD model speed with $-\phi_i = \phi_e = \pi/6$ is $D_0 = 7.429$ mm/μs. Figure 6 shows a comparison of experimental and DSD model diameter chord arrival time fields. The DSD model prediction is good for both speed and arrival times.

4 Summary

We have examined how an annular cylinder geometry affects detonation propagation in the TATB-based high explosive PBX 9502. Detonation shock dynamics modeling was used to explore the effects of

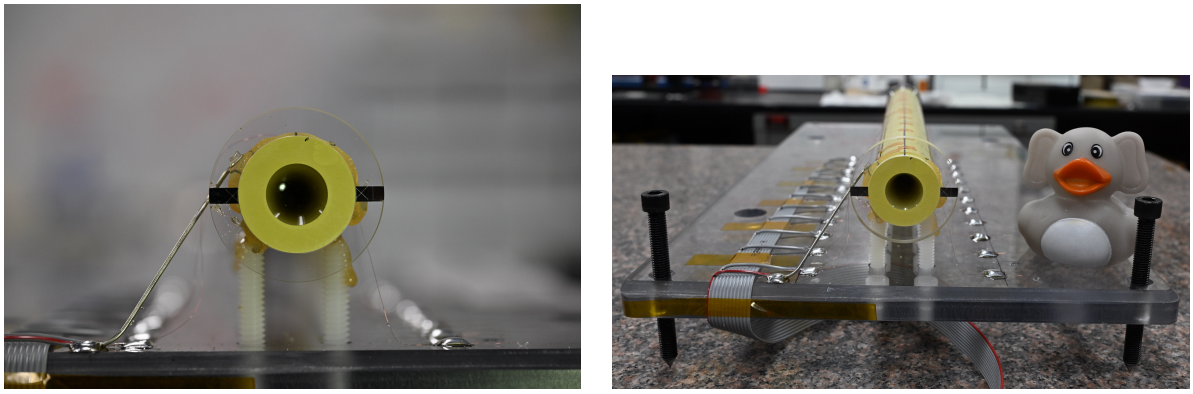

Figure 5: PBX 9502 annular cylinder experiment with $R_i = 6.73$ mm and $R_e = 12.71$ mm.

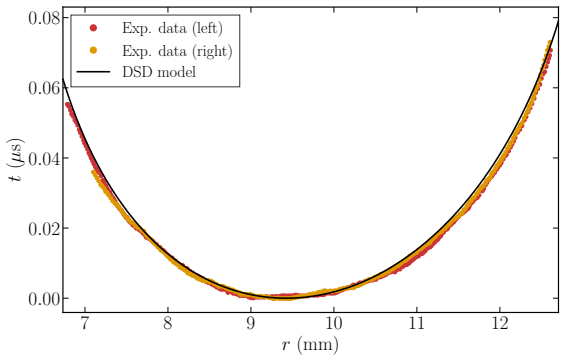

Figure 6: Experimental and DSD model diameter chord arrival time fields. The arrival time field for the left region of the annulus has been reflected about the origin and shown with the right field.

variations in radii and confinement. A validation experiment was conducted that demonstrated good predictive capability of the DSD model in the annular cylindrical geometry.

References

[1] W. Fickett and W. C. Davis. *Detonation*. University of California Press, California, 1979.

[2] J.H.S. Lee. *The detonation phenomenon*. Cambridge University Press, 2008.

[3] J.B. Bdzil. Steady-state two-dimensional detonation. *J. Fluid Mech.*, 108:195–226, 1981.

[4] G.J. Sharpe and M. Braithwaite. Steady non-ideal detonations in cylindrical sticks of explosives. *J. Eng. Math.*, 53:39–58, 2005.

[5] M. Short and J.J. Quirk. High explosive detonation-confiner interactions. *Annu. Rev. Fluid Mech.*, 50:215–242, 2018.

[6] M. Short, J.J. Quirk, C. Chiquete, and C.D. Meyer. Detonation propagation in a circular arc: reactive burn modelling. *J. Fluid Mech.*, 835:970–998, 2018.

[7] J.B. Bdzil and D.S. Stewart. The dynamics of detonation in explosive systems. *Annu. Rev. Fluid Mech.*, 39:263–292, 2007.

[8] S.I. Jackson and M. Short. Scaling of detonation velocity in cylinder and slab geometries for ideal, insensitive and non-ideal explosives. *J. Fluid Mech.*, 773:224–266, 2015.

[9] M. Short, J.J. Quirk, C.D. Meyer, and C. Chiquete. Steady detonation propagation in a circular arc: a Detonation Shock Dynamics model. *J. Fluid Mech.*, 807:87–134, 2016.

[10] D.M. Dattelbaum and L.L. Stevens. Equations of state of binders and related polymers. In *Static Compression of Energetic Materials*, pages 127–202. Springer, 2009.

[11] E.K. Anderson, M. Short, S.J. Voelkel, G.A. Montoya, R.I. Chicas, and C. Chiquete. Influence of initial density on detonation propagation in a TATB-based high explosive. *Combust. Flame*, 273:113920, 2025.

[12] E.K. Anderson, M. Short, S.J. Voelkel, C. Chiquete, R.I. Chicas, and J.R. Gibson. Experimental investigation of high explosive detonation structure and dynamics near the failure diameter. *Proc. Combust. Instit.*, 40:105320, 2024.

[13] M. Short, C. Chiquete, J.B Bdzil, and J.J. Quirk. Detonation diffraction in a circular arc geometry of the insensitive high explosive PBX 9502. *Combust. Flame*, 196:129–143, 2018.

[14] S.J. Voelkel, E.K. Anderson, M. Short, C. Chiquete, and S.I. Jackson. Effect of microstructure on detonation performance of the triaminotrinitrobenzene (TATB)-based insensitive high explosive PBX 9502. *Combust. Flame,*, 246:112373, 2022.